TMEM16A(a)/anoctamin-1 Shares a Homodimeric Architecture with CLC Chloride Channels*⑤

Ghada Fallah‡, Thomas Römer‡, Silvia Detro-Dassen‡, Ursula Braam‡, Fritz Markwardt§, and Günther Schmalzing‡¶

TMEM16A/anoctamin-1 has been identified as a protein with the classic properties of a Ca^{2+}-activated chloride channel. Here, we used blue native polyacrylamide gel electrophoresis (BN-PAGE) and chemical cross-linking to assess the quaternary structure of the mouse TMEM16A(a) and TMEM16A(ac) splice variants as well as a genetically concatenated TMEM16A(a) homodimer. The constructs carried hexahistidyl (His) tags to allow for their purification using a nondenaturing metal affinity resin. Neither His-tagging nor head-to-tail concatenation of two copies of TMEM16A(a) noticeably affected Ca^{2+}-induced measured macroscopic Cl^- currents compared with the wild-type TMEM16A(a) channel. The digitonin-solubilized, nondenatured TMEM16A(a) protein migrated in the BN-PAGE gel as a homodimer, as judged by comparison with the concatenated TMEM16A(a) homodimer and channel proteins of known oligomeric structures (*e.g.* the voltage-gated Cl^- channel CLC-1). Cross-linking with glutaraldehyde corroborated the homodimeric structure of TMEM16A(a). The TMEM16A(a) homodimer detected in *Xenopus laevis* oocytes and HEK 293 cells dissociated into monomers following denaturation with SDS, and reducing *versus* nonreducing SDS-PAGE provided no evidence for the presence of intersubunit disulfide bonds. Together, our data demonstrate that the Ca^{2+}-activated chloride channel member TMEM16A shares an obligate homodimeric architecture with the hCLC-1 channel. *Molecular & Cellular Proteomics 10: 10.1074/mcp.M110.004697, 1–10, 2011.*

Ca^{2+}-activated Cl^- channels (CaCCs)[1], which are activated by intracellular Ca^{2+} at submicromolar and low micromolar concentrations, were first identified in *Xenopus laevis* oocytes (1, 2), where they generate the fertilization potential that provides a fast electrical block to prevent polyspermy (3). CaCCs have been found in a wide range of organisms and tissues and are implicated in important physiological processes, including vascular smooth-muscle contraction, cell-volume regulation, electrolyte secretion, and the regulation of neuron excitability (4). All CaCCs possess similar biophysical characteristics, including a small single-channel conductance, voltage-dependent Ca^{2+} sensitivity, and a characteristic halide-permeability sequence ($I^- > Br^- > Cl^- > F^-$). In oocytes, CaCC-mediated currents are mostly outwardly directed (reflecting inward Cl^- movement), because activation of the current normally occurs at potentials more positive than the Cl^- equilibrium potential (5). The CaCC currents continuously report the free ambient Ca^{2+} levels immediately below the plasma membrane (6, 7). CaCC-activating stimuli include Ca^{2+} influx from the extracellular space through voltage-gated Ca^{2+} channels opened by oocyte depolarization to potentials around 0 mV (1), Ca^{2+} released from intracellular IP_3-sensitive Ca^{2+} stores (8), or intracellular Ca^{2+} injection (5, 9). Indeed, voltage-clamp recordings of endogenous CaCC currents are a convenient reporter of the functioning of either endogenous or ectopically expressed G-protein-coupled receptors that stimulate Ca^{2+} release through the inositol phospholipid messenger pathway upon activation (10–12).

Although the molecular identity of CaCCs was unknown until recently, three independent studies using different strategies identified TMEM16A as a protein with classic CaCC properties (13–15). The TMEM16 family includes ten members (designated A through K) that share a common topology, including long intracellular N- and C-terminal tails and eight membrane-spanning segments (designated M1 to M8) that are connected by intervening loops (Fig. 1*A*). Because of their role in anion transport and their eight-transmembrane, helical topology, TMEM16 proteins are also designated as anoctamins (15). Further diversity in the TMEM16A isoform arises from tissue-specific alternative splicing of three exons: 6b, 13, and 15 (corresponding to

[1] The abbreviations used are: CaCC, Ca^{2+}-activated chloride channel; BN-PAGE, blue native PAGE; CLC, voltage-gated chloride channel; Cy5 NHS ester, cyanine 5 N-hydroxysulfosuccinimide ester; Endo H, endoglycosidase H; GlyR, glycine-activated receptor; $5HT_3R$, mouse serotonin type 3 receptor; Ni-NTA, nickel-nitrilo acetic acid; ORi, frog Ringer's solution; PNGase F, Peptide: N-Glycosidase F; TEVC, two-electrode voltage-clamp; His, hexahistidyl; DTT, dithiotreitol.
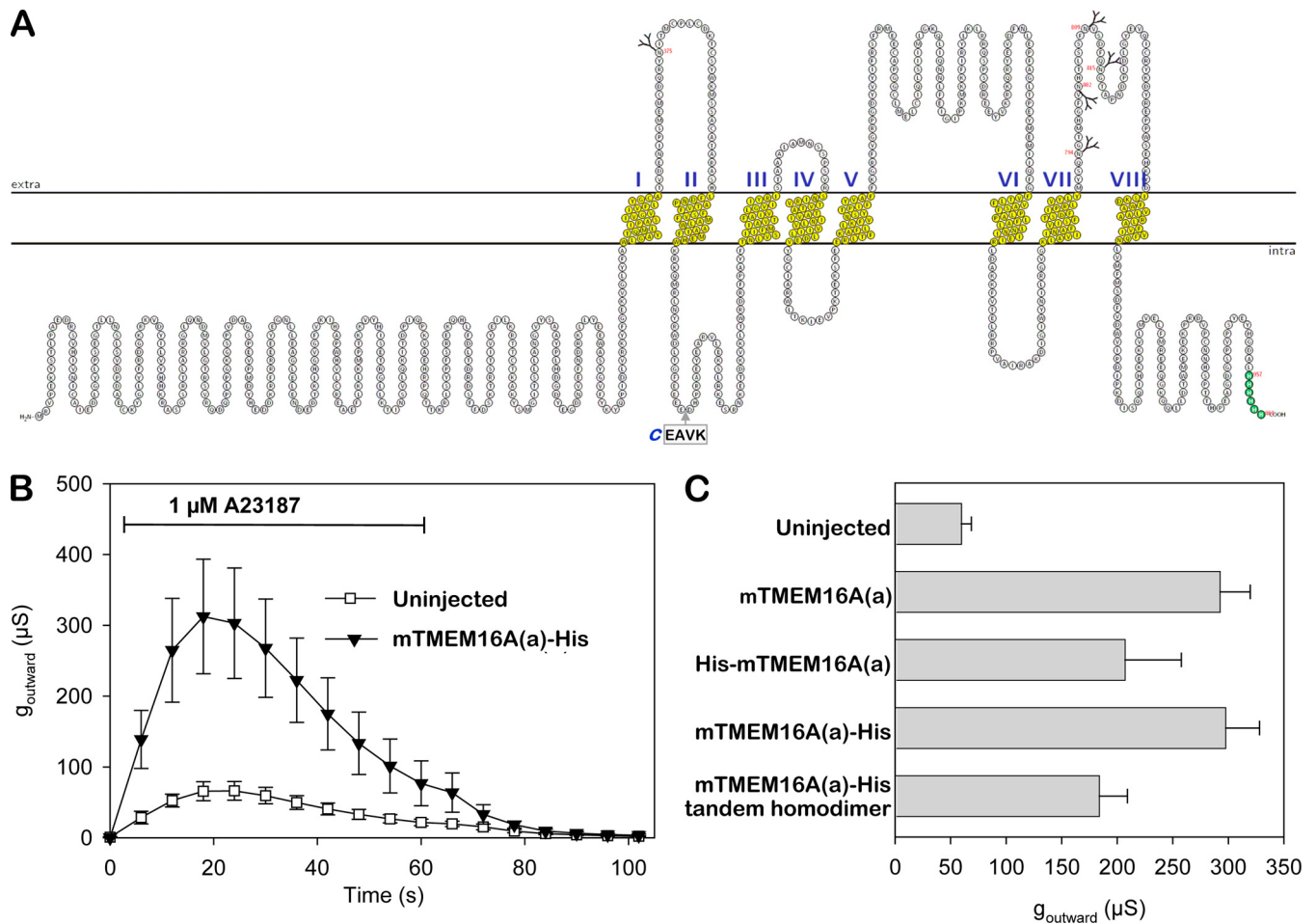
FIG. 1. **Functional characterization of mTMEM16A(a) in *X. laevis* oocytes.** *A*, Topological model of mTMEM16A, as drawn with TeXtopo (44). The indicated location of the transmembrane segments (TMI-TMVIII) was calculated with the topology prediction program MEMSAT3.0 (56). The C-terminal His tag (*green*) and the positions of the five luminally located *N*-glycosylation sequons (NXS/T) are also indicated. Human TMEM16A(a) isoforms are generated by the inclusion or omission of three alternative segments, *b-d* (14), of which the sequence of segment *c* (EAVK) was identified in the mouse genome following a BLAST search of DNA databases. *B*, Current responses were elicited in uninjected control oocytes and mTMEM16A(a)-expressing oocytes by the addition of 1 μM A23187 for the time indicated by the horizontal bar. The time-dependent outward conductances are the mean $\pm$ S.E. of recordings from five to six oocytes per data point. *C*, The bars represent the mean $\pm$ S.E. (5 to 17 oocytes per bar) of the maximum outward conductance from the A23187-elicited current response in oocytes expressing the indicated mTMEM16A(a) constructs, recorded as in B.

22-, 4-, and 26-residue stretches, respectively, all located in the cytoplasm) (16). The removal of exons 6b or 13 results in an approximately fourfold increase in Ca^{2+} sensitivity or a change in the time-dependent CaCC current activation at positive membrane potentials, respectively (16).

Mammalian chloride channels are broadly divided into five classes based on their regulation: (i) cAMP-dependent cystic fibrosis transmembrane-conductance regulators; (ii) CaCCs; (iii) voltage-gated chloride channels (CLCs); (iv) inhibitory ligand-gated chloride channels, *e.g.* γ-aminobutyric acid-activated receptors, and glycine-activated receptors; and (v) volume-regulated chloride channels of unknown molecular identity (4, 17). To date, all investigated chloride channels have displayed an oligomeric organization: homodimeric for CLCs (18–22) and CFTR (23) and obligately pentameric for

γ-aminobutyric acid-activated$_A$ receptors and the glycine-activated receptors (24–26). However, because of the lack of sequence homology to these and other proteins, the possible oligomeric structure of TMEM16A cannot be inferred by analogy. To experimentally determine the higher ordering of TMEM16A, we used blue native polyacrylamide gel electrophoresis (BN-PAGE), which has been shown to reliably determine the quaternary structure of various membrane proteins (25, 27–34) and the scaffolding protein gephyrin (35). We found that functional splicing variants of TMEM16A assemble as homodimers in the endoplasmic reticulum of *X. laevis* oocytes, and these homodimers are efficiently exported to the cell surface. Partial results of this work were presented in a poster at the 24th Annual Symposium of The Protein Society (36).

EXPERIMENTAL PROCEDURES

Expression of Affinity-tagged TMEM16A(a) in X. laevis Oocytes— Throughout this report, we follow the original nomenclature for the human TMEM16A variants to indicate the presence of the alternative exons *a* (116 N-terminal residues) and *c* (four residues) (14). Mouse mTMEM16A(a) cDNA (GenBank accession number NM 178642.4) was subcloned into the pNKS2 oocyte expression vector using Gateway cloning (Invitrogen) (37). A hexahistidyl (His) tag was introduced immediately 3′ or 5′ of the ATG start codon or the stop codon, respectively, to generate His-mTMEM16A(a) and mTMEM16A(a)-His. The splicing variant mTMEM16A(ac)-His was generated by inserting codons encoding the EAVK tetrapeptide (GeneID 101772 Ano1) between the codons for ^{447}E and ^{448}D of mTMEM16A(a)-His. A construct encoding a concatenated homodimer of mTMEM16A(a) was generated by covalently linking two copies of the mTMEM16A(a) cDNA (the first copy without a His tag, the second with a C-terminal His tag) in a single open reading frame to generate (mTMEM16A(a))$_2$-His (34, 38, 39). Oocyte expression plasmids encoding the human-muscle chloride channel hCLC-1, the human hGlyR α1 subunit, and the mouse serotonin type 3 receptor (m5HT$_3$R) have been described previously (25, 34). All mutations and insertions were performed using a QuikChange Site-Directed Mutagenesis Kit (Stratagene, La Jolla, CA) with mutagenic primers that incorporated or removed a silent restriction site. Positive clones were identified using restriction-enzyme analysis, and the DNA sequences were confirmed by sequencing.

*Oocyte Expression and Two-Electrode Voltage-Clamp (TEVC) Electrophysiology—*Collagenase-defolliculated *Xenopus* oocytes (Stage V or VI) were isolated and injected with capped cRNAs, as previously described (27). Oocytes were incubated at 19 °C in sterile frog Ringer's solution (ORi: 90 mM NaCl, 1 mM KCl, 1 mM CaCl$_2$, 1 mM MgCl$_2$, and 10 mM HEPES; pH 7.4) supplemented with 50 mg/l gentamycin. One to 3 days after cRNA injection (23 nl of 0.3 μg/μl cRNA), current responses were recorded with TEVC, as previously described (40). The oocyte membrane potential was held at -40 mV and depolarized every 6 s from -80 to +40 mV within 2 s in a ramplike fashion. To elicit Ca^{2+}-dependent ion currents, the Ca^{2+} ionophore A23187 was added to the ORi bath solution at a final concentration of 1 μM. To test the Ca^{2+} dependence of the response, Ca^{2+} was excluded from the ORi bath solution and 0.1 mM EGTA was added. To analyze the permeation behavior of the A23187-induced currents, Na$^+$ or Cl$^-$ was replaced with Tris$^+$ or glutamate, respectively. For the experiments in low-chloride (4.5 mM Cl$^-$) medium, we connected the bath electrodes to the extracellular solution via 3 M KCl-agar bridges to avoid voltage offsets associated with bath-solution changes. The A23187-induced ramp currents were calculated by subtracting the average of three to five ramp currents measured before the addition of A23187 from those measured during A23187 addition. The outwardly directed ramp conductance was determined by linear approximation of the ramp currents in the +20 to +40 mV voltage range.

*Protein Labeling, Purification, and PAGE—*cRNA-injected oocytes were metabolically labeled by overnight incubation with L-[^{35}S]-methionine and surface-labeled with cyanine 5 (Cy5) NHS ester (an amine-reactive, membrane-impermeable fluorescent dye) just prior to protein extraction, as previously described (41). His-tagged proteins were purified by nickel-nitrilo acetic acid (Ni-NTA) agarose (Qiagen) chromatography from digitonin (1%, w/v) oocyte extracts, as previously detailed (27, 30). BN-PAGE (42) was performed immediately after protein purification (27) in the presence of 0.02% (w/v) Coomassie blue G250, as described. Where indicated, the samples were treated with 100 mM dithiothreitol (DTT), 0.001%–0.1% (w/v) SDS, or a combination of both for 1 h at 37 °C prior to BN-PAGE to induce partial dissociation of the channel complexes. During electrophoresis, the BN-PAGE gel becomes strongly stained by the Coomassie G250 dye, and this intense staining completely extinguishes the fluores-

cence of the protein-bound Cy5. Therefore, BN-PAGE gels were first destained by repeated cycles of incubation in 50% v/v acetonitrile (Biosolve, Valkenswaard, Netherlands) supplemented with 25 mM ammonium carbonate, following a previously described protocol (43). After complete destaining, the acetonitrile mixture was replaced by several washes with 0.1 M sodium phosphate buffer, pH 8.0, and the gel was scanned wet in a Typhoon scanner (GE Healthcare). For the subsequent visualization of ^{35}S-labeled proteins, the BN-PAGE gels were dried, exposed to a phosphor screen, and scanned on a PhosphorImager (Storm 820, GE Healthcare).

For SDS-urea PAGE, we mixed the samples with SDS sample buffer in the presence or absence of 20 mM DTT, as indicated, and electrophoresed them in parallel with [^{14}C]-labeled molecular-mass markers (Rainbow, Amersham Biosciences) in linear or gradient polyacrylamide gels. To investigate the glycosylation state of the proteins, samples were treated with either endoglycosidase H (Endo H) or PNGase F (New England Biolabs, Beverly, MA) for 2 h in the presence of reducing SDS sample buffer and 1% (w/v) Nonidet P40 to counteract the SDS-mediated inactivation of PNGase F. After SDS-PAGE, we directly scanned the wet tricine gels on a fluorescence scanner (Typhoon, GE Healthcare) to visualize the fluorescently labeled plasma membrane-bound proteins and then dried the gels for the subsequent detection of ^{35}S incorporation as described above.

*Chemical Cross-linking—*cRNA-injected *X. laevis* oocytes were metabolically labeled overnight with [^{35}S]-methionine, chased for 24 h, and then surface-labeled with Cy5 NHS ester for 30 min. The cross-linking reaction was then immediately initiated by homogenizing the intact oocytes in 100 mM sodium phosphate buffer, pH 8.0, and 1% (w/v) digitonin supplemented with the indicated concentration of dimethyl adipimidate (Pierce) or glutaraldehyde (Roth Chemicals, Karlsruhe, Germany). The reaction was allowed to proceed for 30 min at 21–23 °C with continuous horizontal shaking and terminated by the addition of Tris/HCl, pH 8.0, to a final concentration of 0.1 M to quench excess cross-linker. The proteins were then affinity purified by nondenaturing Ni-NTA chromatography, as described previously (27, 30).

*Generation of a HEK 293 Cell Line Stably Expressing the mTMEM16A(ac) Channel—*The mTMEM16A(ac) coding sequence was subcloned into the pcDNA5/FRT/TO inducible expression vector using the Gateway cloning system, following the manufacturer's instructions (Invitrogen, Karlsruhe, Germany), to generate a stable Flp-In HEK 293 cell line. Expression was induced in the cells by the addition of 1 μg/ml tetracycline for 36 h. The cells were then surface labeled with Cy5-NHS ester for 30 min at 21–23 °C and quenched with 20 mM glycine for 5 min, and proteins were extracted using digitonin (0.5%, w/v) in phosphate-buffered saline, pH 8.0. The tagged proteins were purified using Ni-NTA resin, washed, eluted in nondenaturing imidazole buffer, and subjected to SDS-PAGE and BN-PAGE as described above. In the indicated experiments, the digitonin was replaced with 0.01% (w/v) and 0.03% (w/v) dodecyl maltoside (Biomol, Germany) for protein extraction and nondenaturing elution, respectively.

*Data Analysis—*The intensity of the protein bands was quantified using the ImageQuant TL software version 7.0 (GE Healthcare Biosciences). Figures with halftone images were prepared with ImageQuant TL for contrast adjustments, Adobe Photoshop CS 8.0 for level adjustment and cropping, and Microsoft PowerPoint 2000 for labeling. The topology map was drawn with T$_E$Xtopo (44). The data were analyzed using a one-way analysis of variance (ANOVA; $p < 0.05$) and are presented as the mean $\pm$ S.E. All line and bar graphs were prepared using SigmaPlot 8.0 (Systat Software, San Jose, CA, USA). Each experiment was performed at least three times with equivalent results.
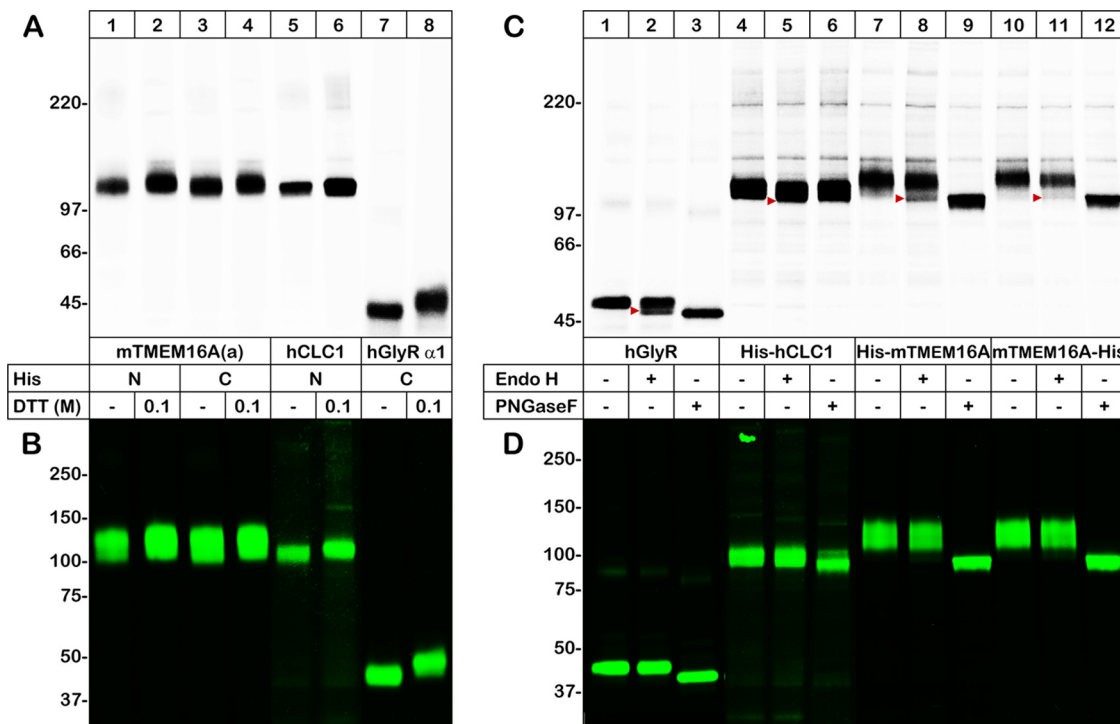
FIG. 2. **Total and cell-surface expression of the Cl⁻-conducting channels mTMEM16A(a), hCLC-1, and hGlyR α1.** *A, B,* The indicated [^{35}S]-methionine- and Cy5-labeled proteins were purified by Ni-NTA chromatography and resolved with both reducing and nonreducing SDS-urea-PAGE. The incorporated [^{35}S]-methionine (*A*) and Cy5 fluorescence (*B*) was visualized with phosphorimaging and Typhoon fluorescence scanning to display the total and cell-surface pools of the proteins, respectively. N and C in the figure legend indicate whether the His tag was N- or C-terminally positioned, respectively. *C, D,* Aliquots of the same protein samples used in *A* and *B* were deglycosylated with Endo H and PNGase F, as indicated, and were found to exist exclusively in the complex-glycosylated form in the plasma membrane (*D*). In contrast, the [^{35}S]-methionine-labeled protein was partially Endo H-sensitive (*C*, red arrowheads).

RESULTS

Both *X. laevis* oocytes and HEK 293 cells were used to express the various mTMEM16A(a) constructs, all of which encoded a hexahistidine tag for one-step affinity purification. After metabolic and/or cell-surface labeling with [^{35}S]-methionine and/or the covalently bound fluorescent Cy5 dye, respectively, proteins were extracted with the mild nonionic detergent digitonin in the presence of iodoacetamide to preserve noncovalent protein-protein interactions and to prevent artifactual intersubunit cross-linking by disulfide bonds, respectively. The mTMEM16A(a) proteins were affinity-purified on a Ni-affinity resin, eluted in nondenaturing buffer, and analyzed using nonreducing SDS-PAGE, BN-PAGE, and chemical cross-linking to determine their oligomeric state. Additionally, the oocyte-expressed constructs were tested functionally with TEVC electrophysiology.

N- or C-terminally His-tagged mTMEM16A(a) and a Tandem mTMEM16A(a) Homodimer are Functional in X. laevis Oocytes—To examine whether an N- or C-terminally positioned His-tag affects the function of mTMEM16A(a), TEVC measurements were performed. Increasing the intracellular Ca^{2+} concentration of intact oocytes by the addition of the Ca^{2+} ionophore A23187 induced transient outward currents that were approximately fivefold greater in mTMEM16A(a)-ex-

pressing oocytes than in uninjected control oocytes (Fig. 1*B*). The A23187-induced maximum outward conductances were statistically similar among the oocytes expressing the various mTMEM16A(a) constructs, including the wild-type mTMEM16A(a) and the mTMEM16A(a)-His tandem homodimer (Fig. 1*C*). On the basis of these results, tagging the N- or C terminus of mTMEM16A(a) with a hexahistidyl sequence or genetically concatenating two mTMEM16A(a) copies in a head-to-tail fashion does not adversely affect the Ca^{2+}-gated Cl⁻ channel function of mTMEM16A(a).

The A23187-induced outward conductance in mTMEM16A(a)-expressing oocytes was reduced in Ca^{2+}-free or glutamate-based low Cl⁻ bathing solution. Also, the reversal potential (≈ -10 mV in ORi bath solution) shifted by +50 mV when Cl⁻ was replaced by glutamate (data not shown). Replacing Na$^+$ with Tris$^+$ did not significantly change the outward conductance or the reversal potential (data not shown). These results are in line with the induction of a Ca^{2+}-dependent Cl⁻ current.

mTMEM16A(a) Does Not Form Disulfide-linked Oligomers and is Efficiently Exported to the Plasma Membrane as a Complex-type Glycoprotein—The freshly isolated [^{35}S]-methionine-labeled mTMEM16A(a) subunit (956 amino acids) tagged with either an N- or a C-terminal His-tag migrated in 4%–10% nonreducing SDS-urea-PAGE gradient gels as a

single band with a molecular mass of ~120 kDa (Fig. 2*A*, lanes 1 and 3), which is in agreement with the sequence-predicted 110-kDa protein core (excluding the His-tag and carbohydrates). Reduction with DTT resulted in a small increase in the apparent molecular mass of the mTMEM16A(a) polypeptide (Fig. 2*A*, lanes 2 and 4) compared with the oxidized form (Fig. 2*A*, lanes 1 and 3). Although this small shift may have resulted from the reduction of intrasubunit disulfide bonds, the absence of a large decrease in the molecular mass clearly indicates the absence of intersubunit disulfide bonds. A faint, ~250-kDa band (suggestive of a homodimer resistant to both SDS and DTT) could only be detected at extremely high image intensity settings (data not shown). However, following storage of the isolated proteins for one or more days, the intensity of the 250-kDa band increased significantly (data not shown). Therefore, we only show data obtained with proteins analyzed on the day of their purification, with the sole exception of the deglycosylation experiments, which were performed on older proteins.

In their nonreduced forms, the analyzed His-hCLC-1 and hGlyR α1 protomers migrated as 113-kDa (Fig. 2*A*, lane 5) and 42-kDa (Fig. 2*A*, lane 7) bands, respectively, which is close to the masses of their sequence-predicted protein cores (110 kDa and 39 kDa). As with mTMEM16A(a), reduction with DTT slightly reduced the apparent mass of the hCLC-1 and the hGlyR α1 protomers (Fig. 2*A*, lane 8); disulfide-linked multimers were not detected in the freshly purified protein samples.

All three proteins (mTMEM16A(a), hCLC-1, and hGlyR α1) were incorporated into the oocyte plasma membrane, as illustrated by the Cy5 fluorescence, which was covalently linked to lysine residues that were accessible on the external oocyte surface when the intact oocytes were incubated with Cy5 NHS ester prior to affinity purification (Fig. 2*B*). Although the mTMEM16A(a) channel and hGlyR α1 exhibited relatively strong Cy5 fluorescence (Fig. 2*B*, lanes 1–4 and 7–8), an 8-fold higher image gain setting was required to visualize the Cy5-labeled hCLC-1 channel (Fig. 2*B*, lanes 5–6). This low fluorescence may reflect less efficient incorporation of the hCLC-1 channel into the plasma membrane and/or a lower number of cell surface-exposed lysine residues that were accessible for the labeling reaction. Similar to the above results, at the plasma membrane level, none of the three chloride channels existed as disulfide-linked oligomers.

As detected following deglycosylation with Endo H and PNGase F, 67 and 87% of the total ^{35}S-labeled His-mTMEM16A(a) and mTMEM16A(a)-His subunits, respectively, were in the mature complex-glycosylated form (Fig. 2*C*, lanes 8 and 11), indicating efficient egress from the ER to the Golgi and later compartments. Only the complex-glycosylated form of His-mTMEM16A(a) (Fig. 2*D*, lanes 7–9) and mTMEM16A(a)-His (Fig. 2*D*, lanes 10–12) reached the plasma membrane, similar to the hGlyR α1-His (Fig. 2*D*, lanes 1–3) and His-hCLC-1 (Fig. 2*D*, lanes 4–6) anion channels.

Deglycosylation with PNGase F reduced the average molecular mass of the mature mTMEM16A(a) subunit by ~17 kDa (Figs. 2*C* and 2*D*, lanes 9 and 12). Because of the heterogeneity of complex-type carbohydrates, the mass of individual complex-type *N*-glycans is unknown, and thus, their number cannot be ascertained from the size of the mass shift. Therefore, we purified the mTMEM16A(a) protein directly following a 4-h ^{35}S-methionine pulse, when virtually all *N*-glycans on the ^{35}S-methionine-labeled proteins are still in the uniform high-mannose form, each adding ~3 kDa to the protein core. Deglycosylation of the mTMEM16A(a) polypeptide with Endo H resulted in an ~9-kDa shift (data not shown), suggestive of the removal of three 3-kDa *N*-glycans. To determine whether [375]N was a putative *N*-glycan acceptor site, we mutated [375]N to glutamine (see Fig. 1*A*). This mutation resulted in a 3-kDa decrease in the molecular mass of the high-mannose form of mTMEM16A(a), thereby verifying [375]N as one of the several *N*-glycosylation sites (data not shown).

In contrast, no change in the molecular mass was observed when we mutated [591]N, which is located in the extracellular TM3-TM4 loop, to glutamine (data not shown), indicating that [591]N is not glycosylated. Both the *N*-glycosylation-blocking proline residue present at the +4 position of the [591]NSSP sequence and the relatively short distance to the membrane (Fig. 1*A*) are sufficient restraints to prevent the *N*-glycosylation of [591]N. Together, these data suggest that the mTMEM16A(a) protomer contains one *N*-glycan in the extracellular TM1-TM2 loop and at least two additional *N*-glycans in the TM7-TM8 ectoloop, where four NXS/T sequons are present (see Fig. 1*A* for the position of these residues). Two *N*-glycans have also been detected in the TM7-TM8 ectoloop of anoctamin-7 at sequons [809]NFT and [824]NRT (45), which correspond to [802]NHT and [815]NGT of mTMEM16A(a), respectively.

mTMEM16A(a) and mTMEM16A(ac) Migrate as Discrete Homodimers in BN-PAGE—To determine the higher-order structure of TMEM16A(a), we analyzed the protein purified under native conditions with BN-PAGE. As positive controls, we coanalyzed two chloride channels of known quaternary structure (the homopentameric hGlyR α1 and the homodimeric hCLC-1) and one cation channel, the homopentameric m5HT$_3$R. In addition, we used hGlyR α1 and m5HT$_3$R as well as their well-defined lower-ordered intermediates generated by partial denaturation as reliable molecular-mass markers for the determination of the mass of the assembled and SDS-disassembled mTMEM16A(a). By substituting these well-defined membrane proteins for the common soluble calibration proteins, the errors that arise when estimating the mass of membrane proteins by comparison with soluble proteins are avoided (27, 39, 46). Nondenatured mTMEM16A(a) (Fig. 3*A*, lanes 3 and 9) migrated as a distinct band in the BN-PAGE gel to the same position as the ~320-kDa m5HT$_3$R (Fig. 3*A*, lane 15; 64 kDa per triglycosylated protomer) and with a somewhat higher mass than the ~260-kDa hGlyR α1
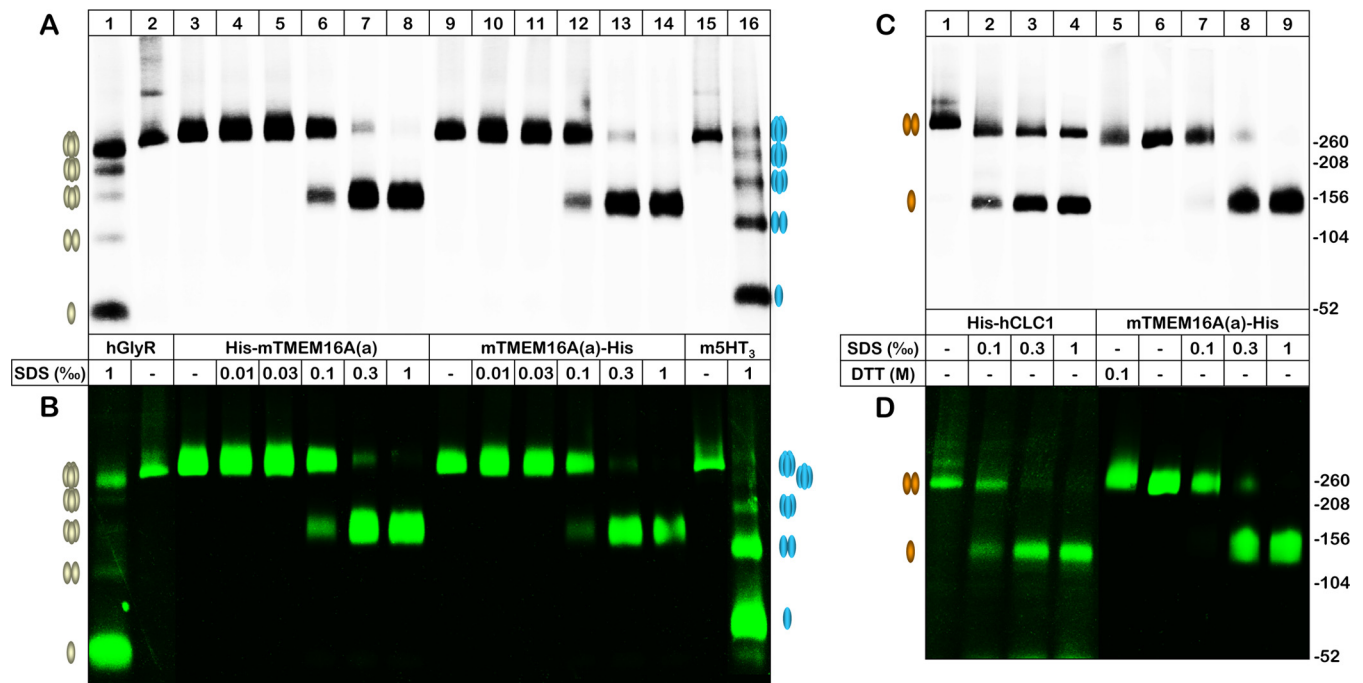
FIG. 3. **BN-PAGE analysis of the oligomeric structure of mTMEM16A(a).** The indicated channel proteins were purified by nondenaturing Ni-NTA chromatography from digitonin extracts of *X. laevis* oocytes, resolved by BN-PAGE, and visualized in the [^{35}S]-methionine-labeled total form or the Cy5-labeled plasma membrane-bound form with phosphorimaging (upper panels) or Typhoon fluorescence scanning (lower panels), respectively. Protein migration is shown both under native conditions and after partial denaturation following a 1-h incubation with SDS and/or DTT at 37 °C, as indicated. *A*, *B*, The yellow and blue ovals schematically illustrate the oligomeric states (protomers to pentamers) of the partially denatured hGlyR α1 and m5HT$_3$R, respectively. *C*, *D*, The orange ovals schematically illustrate the native homodimeric and the denatured protomeric states of the hCLC-1 channel; the homodimeric structure of prokaryotic CLCs was verified by x-ray crystallography (54). The number in the right margin indicates the mass of the partially disassembled hGlyR α1, which resolved in the BN-PAGE gel as a ladder of proteins consisting of one to five 52-kDa protomers (cf. Figs. 3*A* and 3*B*, lane 1).

(Fig. 3*A*, lane 2; 52 kDa per monoglycosylated protomer). Note that all three proteins migrated as single, well-defined oligomeric complexes and that higher-order aggregates were almost completely absent.

To determine the number of protomers incorporated in the mTMEM16A(a) channel, we weakened the noncovalent subunit interactions by treating the natively purified, nonreduced protein with increasing concentrations of SDS. Incubation with 0.01% to 0.1% SDS resulted in the partial or complete disappearance of the 320-kDa mTMEM16A(a) band and the appearance of a faster migrating band (Fig. 3*A* and *B*, lanes 6–8 and 12–14). Upon a similar SDS denaturation, hGlyR α1 (Fig. 3*A* and *B*, lane 1) and m5HT$_3$R disassembled into homotetramers, homotrimers, homodimers, and protomers (Fig. 3*A* and *B*, lane 16), consistent with their well-known homopentameric nature. Using the homodimers and homotrimers of hGlyR α1 (Fig. 3*A* and *B*, lane 1) and m5HT$_3$R (Fig. 3*A* and *B*, lane 16) as molecular-mass markers, we determined that the SDS-disassembled mTMEM16A(a) protein in the BN-PAGE gel had an apparent molecular mass of ~150 kDa (Fig. 3*A* and *B*, lanes 6–8 and 12–14). Because no faster migrating band was observed, it is likely that the 150-kDa band corresponds to the mTMEM16A(a) protomer, which migrates at ~130 kDa in a standard SDS-PAGE gel. The differ-

ence in the molecular masses indicated by SDS-PAGE and BN-PAGE is likely be because of the different separation principles of the two methods, *i.e.* charge-to-mass ratio and protein size, respectively (42).

As an additional positive control, we analyzed the hCLC-1 channel in parallel with the mTMEM16A(a) channel by BN-PAGE. In the nondenatured state, the homodimeric hCLC-1 channel migrated to a similar position in the BN-PAGE gel as the mTMEM16A(a) channel (Figs. 3*C* and 3*D*, compare lanes 1 and 6), indicating a similar molecular mass. Disassembly of the hCLC-1 complex with SDS resulted in the appearance of one smaller protein band (Figs. 3*C* and 3*D*, lanes 2–4) that comigrated with the SDS-disassembled mTMEM16A(a) protein in the BN-PAGE gel (Figs. 3*C* and 3*D*, lanes 8–9). Because the hCLC-1 protomer and the mTMEM16A(a) protomer share a similar molecular mass, their identical migration pattern in both the nondenatured and denatured states suggests that the mTMEM16A(a) channel and the hCLC-1 channel also share a homodimeric structure.

Human TMEM16A exists as several splicing variants that differ in the presence of the alternative exons *b* (22 codons), *c* (4 codons), or *d* (26 codons) (14). Using a BLAST search, we identified a mTMEM16A(ac) sequence that shares an exon *c*-encoded EAVK sequence identical to the human
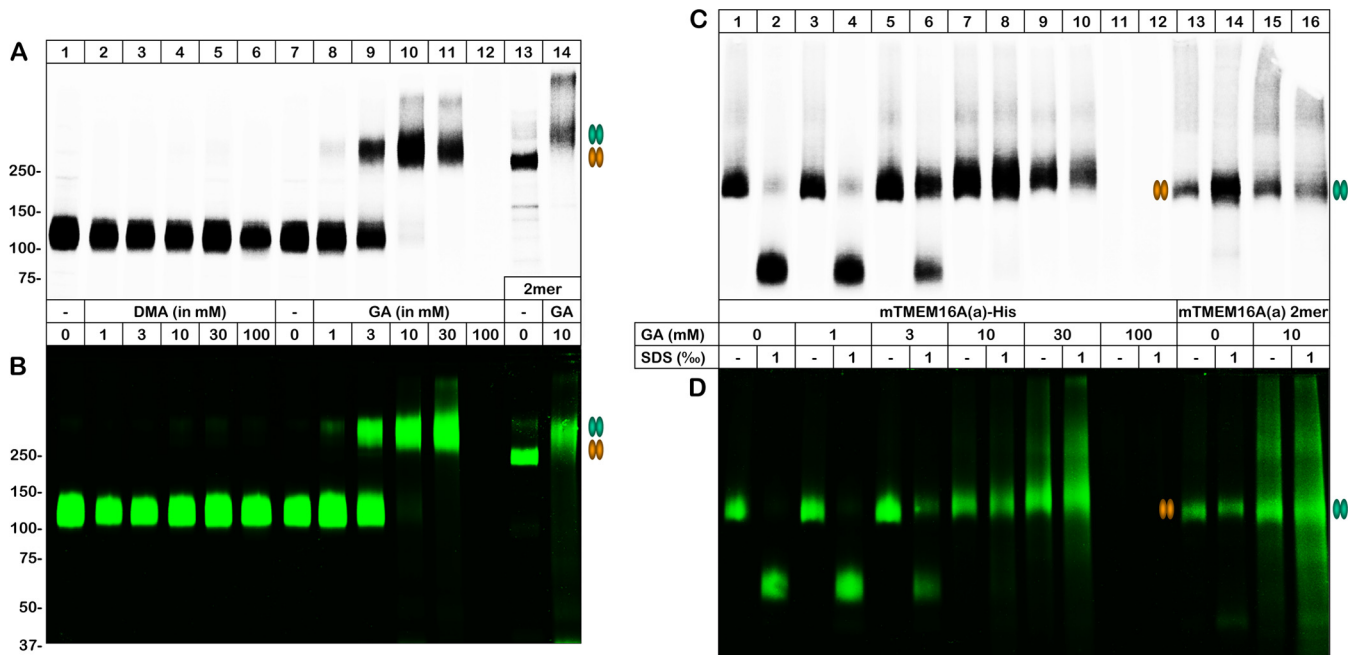
FIG. 4. **Analysis of the oligomeric structure of mTMEM16A(a) following chemical cross-linking.** mTMEM16A(a)-expressing *X. laevis* oocytes were metabolically labeled with [^{35}S]-methionine overnight. After an additional 24-h chase, the outer oocyte surface was labeled with Cy5-NHS-ester. Immediately thereafter, the oocytes were homogenized in the presence of the indicated concentration of dimethyl adipimidate (DMA) or glutaraldehyde (GA). The proteins were purified by nondenaturing Ni-NTA chromatography and resolved in the fully SDS-denatured state with reducing SDS-urea-PAGE (*A, B*) and in the nondenatured and partially SDS-denatured state with BN-PAGE (*C, D*). The upper and lower panels present the [^{35}S]-methionine-labeled total form and the Cy5-labeled plasma membrane-bound form of the polypeptides. Note that no protein could be isolated following treatment with 100 mM glutaraldehyde. The concatenated mTMEM16A(a) dimer was also analyzed. The orange and green double ovals indicate the position(s) of the concatenated mTMEM16A(a) homodimer following no treatment or treatment with 10 mM glutaraldehyde, respectively. Lanes 12–14 were taken at threefold higher image gain settings than the other lanes.

TMEM16A(ac). Therefore, we inserted the four exon *c* codons (Fig. 1*A*) to generate an mTMEM16A(ac)-His-encoding construct. Following BN-PAGE, the nondenatured mTMEM16A(ac)-His protein migrated to the same position (Supplemental Figs. 1*A* and 1*B*, lane 1) as the mTMEM16A(a)-His protein (Supplemental Figs. 1*A* and 1*B*, lane 3), indicating that the EAVK insertion had no obvious effect on the oligomeric state. Additionally, the cell-surface abundances of mTMEM16A(a) (Supplemental Fig. 1*C*, lane 2) and mTMEM16A(ac) (Supplemental Fig. 1*C*, lane 1) were not noticeably different.

To unequivocally define the migration position of the mTMEM16A(a) homodimer, we analyzed a concatenated mTMEM16A(a)-His homodimer encoded by two mTMEM16A(a) monomers joined head-to-tail in a single open reading frame. The noncovalently assembled wild-type mTMEM16A(a) protein and the genetically fused mTMEM16A(a)-His tandem homodimer migrated to identical positions in the BN-PAGE gel, strongly corroborating the homodimeric nature of the noncovalently linked wild-type 320-kDa mTMEM16A(a)-His protein (Supplemental Figs. 1*A* and 1*B*, compare lanes 3 and 5). As expected for a covalently linked dimer, the size of the mTMEM16A(a)-His tandem dimer was unaffected by SDS treatment, in contrast to the noncovalently assembled wild-type mTMEM16A(a)-His homodimer,

which readily disassembled into free protomers (Supplemental Figs. 1*A* and 1*B*, compare lanes 4 and 6). Furthermore, the approximately twofold greater molecular mass of the concatenated mTMEM16A(a) homodimer (Supplemental Figs. 1*C* and 1*D*, lane 3) compared with the mTMEM16A(a) protomer (Supplemental Figs. 1*C* and 1*D*, lane 2) is apparent from the SDS-PAGE gel.

Chemical Cross-linking Generates Covalently Linked TMEM16A(a) Dimers—To determine the quaternary structure of TMEM16A(a) whereas it is still incorporated in the natural lipid bilayer, we homogenized mTMEM16A(a)-expressing oocytes following Cy5 surface labeling in the presence of increasing concentrations of chemical cross-linkers. The imidoester dimethyl adipimidate, which has an 8.6-Å spacer arm, failed to generate mTMEM16A(a) oligomers (Figs. 4*A* and 4*B*, lanes 1–6). Next, we used glutaraldehyde, which has a shorter spacer arm length of ~5 Å. Glutaraldehyde exists in multiple forms in aqueous solutions and, similarly to dimethyl adipimidate, generates chemically stable cross-links between the ε-amino group of lysine residues (47). As detected using reducing SDS-urea-PAGE, glutaraldehyde cross-linked the mTMEM16A(a) protein very efficiently into a single higher molecular mass adduct (Figs. 4*A* and 4*B*, lanes 8–11). At 10 and 30 mM glutaraldehyde, very little or no protomer was visible, indicating that mTMEM16A(a) was almost fully fixed in

the higher-order structure (Figs. 4*A* and 4*B*, lanes 10 and 11). We estimated that the apparent molecular mass of the adduct (Figs. 4*A* and 4*B*, lanes 9–11) was 2.4 times that of the mTMEM16A(a) protomer (Figs. 4*A* and 4*B*, lane 7) and 1.2 times that of the concatenated mTMEM16A(a) homodimer (Figs. 4*A* and 4*B*, lane 13), and thus, somewhat larger than expected for a homodimer. It should be noted, however, that the treatment with glutaraldehyde retarded protein mobility in the SDS-PAGE gel to a certain degree, as evidenced by the apparent 20% increase in the mass of the concatenated mTMEM16A(a) homodimer following treatment with 10 mM glutaraldehyde (Figs. 4*A* and 4*B*, lane 14). Indeed, the 10 mM glutaraldehyde-treated concatenated mTMEM16A(a) homodimer (Figs. 4*A* and 4*B*, lane 14) and the mTMEM16A(a) adduct generated by cross-linking with 10 mM glutaraldehyde (Figs. 4*A* and 4*B*, lane 10) migrated to virtually the same position in the BN-PAGE gel. These findings are fully consistent with the view that chemical cross-linking by glutaraldehyde generated homodimeric mTMEM16A(a) adducts. The shift in mass may arise following the glutaraldehyde concentration-dependent formation of mono-linked and loop-linked byproducts of the cross-linking reaction (48).

Further strong support for the homodimeric structure of the glutaraldehyde-cross-linked mTMEM16A(a) protein comes from BN-PAGE analysis (Figs. 4*C* and 4*D*), which showed that glutaraldehyde only marginally affects the migration of the nondenatured mTMEM16A(a) protein (Figs. 4*C* and 4*D*, lanes 1–10). Furthermore, the glutaraldehyde-cross-linked mTMEM16A(a) protein migrated to a similar position as the concatenated mTMEM16A(a) homodimer (Figs. 4*C* and 4*D*, lanes 13 and 15). As expected for a covalently cross-linked protein, partial denaturation with SDS failed to dissociate the mTMEM16A(a) homodimer into the protomer (Figs. 4*C* and 4*D*, lanes 8 and 10). In contrast, without cross-linking or upon incomplete cross-linking at low glutaraldehyde concentrations, efficient SDS-induced dissociation into mTMEM16A(a) protomers occurred (Figs. 4*C* and 4*D*, lanes 2, 4, and 6).

mTMEM16A(ac) is Organized as a Homodimer in HEK 293 Cells—To test whether oligomerization of TMEM16A(ac) is affected by the host-cell type, we purified stably expressed mTMEM16A(ac) from tetracycline-inducible HEK 293 cells. After labeling the outer cell surface with Cy5 NHS ester, the His-tagged mTMEM16A(ac) channel was purified by nondenaturing Ni-NTA chromatography and resolved by BN-PAGE (Supplemental Fig. 2*A*). One discrete protein band was observed (Supplemental Fig. 2*A*, lane 1) that comigrated with nondenatured mTMEM16A(ac) protein from *X. laevis* oocytes (data not shown). Pretreatment with SDS resulted in an SDS concentration-dependent dissociation of the mTMEM16A(ac) homodimer into the protomer. The SDS sensitivities of the mTMEM16A(ac) proteins from *X. laevis* oocytes and HEK 293 cells were virtually identical (cf. Figs. 3*A* and 3*B*, lanes 12–14 and Supplemental Fig. 2*A*, lanes 3–5). We also extracted the

mTMEM16A(ac) protein from HEK 293 cells with dodecyl maltoside and reproducibly observed a significant fraction of the mTMEM16A(ac) protomer, even without obvious denaturation of the protein sample (Supplemental Fig. 2*A*, lanes 6–7).

In addition, we performed cross-linking experiments on HEK 293 cells and observed mTMEM16A(ac) homodimers at glutaraldehyde concentrations similar to those in *X. laevis* oocytes (Supplemental Fig. 2*B*, lanes 1–4). Even when dodecyl maltoside was used for protein extraction, mTMEM16A(ac) could be quantitatively fixed in the homodimeric state by glutaraldehyde cross-linking (Supplemental Fig. 2*B*, lanes 5–6). Whether chemically cross-linked by glutaraldehyde or not, the mTMEM16A(ac) homodimers from HEK 293 cells (Supplemental Fig. 2*C*, lanes 1–6) migrated to the same position in the BN-PAGE gel as the concatenated mTMEM16A(ac) homodimer purified from *X. laevis* oocytes (Supplemental Fig. 2*C*, lane 7). Together, the data obtained using HEK 293 cells are fully consistent with the view that the mTMEM16A(ac) channel is organized as a homodimer.

DISCUSSION

TMEM16A is Organized as an Obligate Homodimer—Our data provide strong evidence that the TMEM16A(a) CaCC and its splicing variant TMEM16A(ac) are organized as relatively stable, noncovalent assemblies of two identical subunits. This conclusion is based on a comparison of the digitonin-solubilized mTMEM16A(a) and mTMEM16A(ac) channels in their nondenatured and denatured states with other channel proteins of known oligomeric structure in BN-PAGE gels. Furthermore, this conclusion is supported by glutaraldehyde cross-linking experiments, and similar results were seen using either *X. laevis* oocytes or HEK 293 cells as the host cell. The homodimeric mTMEM16A assembly could be separated into monomers by destabilizing denaturation with SDS but not by chemical reduction with DTT. This indicates that the subunits are held together by noncovalent interactions. In further support of this finding, the use of reducing *versus* nonreducing SDS-PAGE provided no evidence for intersubunit disulfide bonds. On the basis of the identical homodimeric assembly of both the ER-resident and the plasma membrane-bound TMEM16A(a) protein, the noncovalent homodimerization must have already occurred in the ER. This observation classifies the TMEM16A(a) channel as a permanent or obligate oligomer (*i.e.* a protein that occurs only in the oligomeric state), as is the case for most homodimeric proteins (49) and ion channels in general. This further suggests that the TMEM16A(a) channel stably assembles as the subunits fold.

Although purification with digitonin provided clear evidence for an exclusively homodimeric assembly, we observed a significant fraction of free protomers in the BN-PAGE gel when we purified the mTMEM16A(a) channel using dodecyl maltoside. However, no such protomers were observed when the dodecyl maltoside-based protein extraction was combined with glutaraldehyde cross-linking. Taken together,

these results suggest that dodecyl maltoside partially destabilizes the assembly interface within the mTMEM16A homodimer to enable dissociation of the free protomers unless the dissociation is prevented by intersubunit cross-linking. The destabilization may be related to the observation that certain hydrophobic protein-protein interactions are not as well preserved following extraction with dodecyl maltoside as with digitonin (50). Thus, the existence of free TMEM16A(a) monomers in the living cell appears unlikely.

The Head-to-Tail mTMEM16A(a) Tandem Dimer is Functional—The concatemer strategy was first successfully applied to voltage-gated K$^+$ channels (51) and subsequently extended to other ion channels, primarily to assess their stoichiometry and subunit arrangement (for a review, see (52)). We used the concatenated mTMEM16A(a) homodimer as a molecular-mass marker to corroborate the assignment of the dimeric mTMEM16A(a) protein to the correct band and for functional analysis. The low level of aggregation, the efficient incorporation into the plasma membrane (as judged by the low fraction of Endo H-sensitive glycans), and the efficient mediation of a Ca^{2+}-activated Cl$^-$ current all suggest that the mTMEM16A(a) tandem dimer readily adopts a properly folded conformation similar to the mTMEM16A(a) homodimer assembled from free protomers. In particular, we did not observe the formation of a monomeric byproduct from the expressed mTMEM16A(a) tandem dimer. This result is in contrast to our previous experience with concatemers of other membrane proteins, such as the ATP-gated P2X1 receptor (39), the glutamate transporter from *Escherichia coli*, ecgltP (32), and rat prestin (SLC26A5), a member of the solute-carrier family (34). The expression of concatemers of these proteins was associated with the formation of minute amounts of lower-molecular-weight byproducts (such as monomers and dimers) that functionally coassembled, thereby impairing the interpretation of the functional results. A possible clue to the difference between these concatemers and the mTMEM16A(a) tandem dimer may be the high propensity of the mTMEM16A(a) tandem dimer to fold into a native conformation that is not prone to aggregation. The feature that head-to-tail concatenation does not noticeably affect macroscopic Cl$^-$ currents is shared with CLC channels (21, 22).

mTMEM16A(a)-1 Shares a Homodimeric Architecture with hCLC Chloride Channels—The mTMEM16A(a) and hCLC-1 protomers consist of similar numbers of amino acids (956 and 988, respectively). Because the homodimeric architecture of CLC-type chloride channels is well established (20–22), we consider the migration of the nondenatured and SDS-denatured forms of mTMEM16A(a) and hCLC-1 to almost identical positions in the BN-PAGE gel as an additional strong argument in favor of a shared homodimeric architecture.

CLC proteins function as either CLC channels or as H$^+$/Cl$^-$ exchangers that share a common structural organization (53). An obvious difference in the secondary structure compared

with TMEM16A(a) proteins is that the large cytoplasmic domain of CLC follows the transmembrane segments, whereas it precedes the transmembrane segments in TMEM16A(a). Additionally, the number of transmembrane segments differs significantly between the two proteins. The CLC protomer exhibits a complex topology with two structurally related halves, comprising a total of 16 membrane-embedded α-helices of variable length in a strongly tilted orientation (54). A biochemical analysis of the anoctamin-7 protein supports the existence of eight transmembrane segments, as predicted by hydropathy analysis (45). However, given the limited structural resolution of biochemical topology mapping compared with x-ray crystallographic structures, a more complex arrangement of the membrane-embedded helices of TMEM16A(a) seems possible.

Oligomerization provides different structural and functional advantages to proteins, including protection against denaturation because of a reduced surface area, control over the accessibility and specificity of active sites, and increased diversity in the formation of regulatory complexes (55). In the case of most cation channels, the most important role of oligomerization is the formation of a unique central ion pathway by the circular arrangement of a defined number of protomers. It will be interesting to learn whether each subunit of a TMEM16 homodimer contains its own physically separate Cl$^-$-conducting pore (similar to the CLC channels (54)) or whether the pore is formed at the interface within the homodimer in a manner analogous to cation channels.

¶ Address correspondence to: Abteilung Molekulare Pharmakologie, RWTH Aachen, Wendlingweg 2, 52074 Aachen. Tel.: +49 241 8089130; Fax: +49 241 80 82433; Email: gschmalzing@ukaachen.de.

REFERENCES

1. Miledi, R. (1982) A calcium-dependent transient outward current in *Xenopus laevis* oocytes. *Proc. R. Soc. Lond B Biol. Sci.* **215,** 491–497
2. Barish, M. E. (1983) A transient calcium-dependent chloride current in the immature *Xenopus* oocyte. *J. Physiol.* **342,** 309–325
3. Cross, N. L., and Elinson, R. P. (1980) A fast block to polyspermy in frogs mediated by changes in the membrane potential. *Dev. Biol.* **75,** 187–198
4. Duran, C., Thompson, C. H., Xiao, Q., and Hartzell, H. C. (2010) Chloride channels: often enigmatic, rarely predictable. *Annu. Rev. Physiol.* **72,** 95–121
5. Miledi, R., and Parker, I. (1984) Chloride current induced by injection of calcium into *Xenopus* oocytes. *J. Physiol.* **357,** 173–183
6. Gomez-Hernandez, J. M., Stühmer, W., and Parekh, A. B. (1997) Calcium dependence and distribution of calcium-activated chloride channels in *Xenopus* oocytes. *J. Physiol.* **502,** 569–574
7. Machaca, K., and Hartzell, H. C. (1999) Reversible Ca gradients between the subplasmalemma and cytosol differentially activate Ca-dependent Cl currents. *J. Gen. Physiol.* **113,** 249–266
8. Oron, Y., Dascal, N., Nadler, E., and Lupu, M. (1985) Inositol 1,4,5-trisphosphate mimics muscarinic response in *Xenopus* oocytes. *Nature* **313,** 141–143
9. Dascal, N., Gillo, B., and Lass, Y. (1985) Role of calcium mobilization in mediation of acetylcholine-evoked chloride currents in *Xenopus laevis* oocytes. *J. Physiol.* **366,** 299–313
10. Parker, I., and Miledi, R. (1986) Changes in intracellular calcium and in membrane currents evoked by injection of inositol trisphosphate into

Xenopus oocytes. *Proc. R. Soc. Lond B Biol. Sci.* **228,** 307–315

11. Takahashi, T., Neher, E., and Sakmann, B. (1987) Rat brain serotonin receptors in *Xenopus* oocytes are coupled by intracellular calcium to endogenous channels. *Proc. Natl. Acad. Sci. U.S.A.* **84,** 5063–5067

12. Oosawa, Y., and Yamagishi, S. (1989) Rat brain glutamate receptors activate chloride channels in *Xenopus* oocytes coupled by inositol trisphosphate and Ca^{2+}. *J. Physiol.* **408,** 223–232

13. Schroeder, B. C., Cheng, T., Jan, Y. N., and Jan, L. Y. (2008) Expression cloning of TMEM16A as a calcium-activated chloride channel subunit. *Cell* **134,** 1019–1029

14. Caputo, A., Caci, E., Ferrera, L., Pedemonte, N., Barsanti, C., Sondo, E., Pfeffer, U., Ravazzolo, R., Zegarra-Moran, O., and Galietta, L. J. (2008) TMEM16A, a membrane protein associated with calcium-dependent chloride channel activity. *Science* **322,** 590–594

15. Yang, Y. D., Cho, H., Koo, J. Y., Tak, M. H., Cho, Y., Shim, W. S., Park, S. P., Lee, J., Lee, B., Kim, B. M., Raouf, R., Shin, Y. K., and Oh, U. (2008) TMEM16A confers receptor-activated calcium-dependent chloride conductance. *Nature* **455,** 1210–1215

16. Ferrera, L., Caputo, A., Ubby, I., Bussani, E., Zegarra-Moran, O., Ravazzolo, R., Pagani, F., and Galietta, L. J. (2009) Regulation of TMEM16A chloride channel properties by alternative splicing. *J. Biol. Chem.* **284,** 33360–33368

17. Verkman, A. S., and Galietta, L. J. (2009) Chloride channels as drug targets. *Nat. Rev. Drug Discov.* **8,** 153–171

18. Miller, C., and White, M. M. (1984) Dimeric structure of single chloride channels from Torpedo electroplax. *Proc. Natl. Acad. Sci. U.S.A.* **81,** 2772–2775

19. Middleton, R. E., Pheasant, D. J., and Miller, C. (1994) Purification, reconstitution, and subunit composition of a voltage- gated chloride channel from *Torpedo* electroplax. *Biochemistry* **33,** 13189–13198

20. Middleton, R. E., Pheasant, D. J., and Miller, C. (1996) Homodimeric architecture of a ClC-type chloride ion channel. *Nature* **383,** 337–340

21. Ludewig, U., Pusch, M., and Jentsch, T. J. (1996) Two physically distinct pores in the dimeric ClC-0 chloride channel. *Nature* **383,** 340–343

22. Fahlke, C., Knittle, T., Gurnett, C. A., Campbell, K. P., and George, A. L., Jr. (1997) Subunit stoichiometry of human muscle chloride channels. *J. Gen. Physiol.* **109,** 93–104

23. Vergani, P., Lockless, S. W., Nairn, A. C., and Gadsby, D. C. (2005) CFTR channel opening by ATP-driven tight dimerization of its nucleotide-binding domains. *Nature* **433,** 876–880

24. Langosch, D., Thomas, L., and Betz, H. (1988) Conserved quarternary structure of ligand-gated ion channels: the postsynaptic glycine receptor is a pentamer. *Proc. Natl. Acad. Sci. U.S.A.* **85,** 7394–7398

25. Griffon, N., Büttner, C., Nicke, A., Kuhse, J., Schmalzing, G., and Betz, H. (1999) Molecular determinants of glycine receptor subunit assembly. *EMBO J.* **18,** 4711–4721

26. Nayeem, N., Green, T. P., Martin, I. L., and Barnard, E. A. (1994) Quaternary structure of the native GABA$_A$ receptor determined by electron microscopic image analysis. *J. Neurochem.* **62,** 815–818

27. Nicke, A., Bäumert, H. G., Rettinger, J., Eichele, A., Lambrecht, G., Mutschler, E., and Schmalzing, G. (1998) P2X$_1$ and P2X$_3$ receptors form stable trimers: a novel structural motif of ligand-gated ion channels. *EMBO J.* **17,** 3016–3028

28. Nicke, A., Rettinger, J., Mutschler, E., and Schmalzing, G. (1999) Blue native PAGE as a useful method for the analysis of the assembly of distinct combinations of nicotinic acetylcholine receptor subunits. *J. Recept. Signal. Transduct. Res.* **19,** 493–507

29. Büttner, C., Sadtler, S., Leyendecker, A., Laube, B., Griffon, N., Betz, H., and Schmalzing, G. (2001) Ubiquitination precedes internalization and proteolytic cleavage of plasma membrane-bound glycine receptors. *J. Biol. Chem.* **276,** 42978–42985

30. Sadtler, S., Laube, B., Lashub, A., Nicke, A., Betz, H., and Schmalzing, G. (2003) A basic cluster determines topology of the cytoplasmic M3-M4 loop of the glycine receptor α1 subunit. *J. Biol. Chem.* **278,** 16782–16790

31. Nicke, A., Thurau, H., Sadtler, S., Rettinger, J., and Schmalzing, G. (2004) Assembly of nicotinic α7 subunits in *Xenopus* oocytes is partially blocked at the tetramer level. *FEBS Lett.* **575,** 52–58

32. Gendreau, S., Voswinkel, S., Torres-Salazar, D., Lang, N., Heidtmann, H., Detro-Dassen, S., Schmalzing, G., Hidalgo, P., and Fahlke, C. (2004) A trimeric quaternary structure is conserved in bacterial and human glutamate transporters. *J. Biol. Chem.* **279,** 39505–39512

33. Duckwitz, W., Hausmann, R., Aschrafi, A., and Schmalzing, G. (2006) P2X$_5$

34. Detro-Dassen, S., Schänzler, M., Lauks, H., Martin, I., Zu, Berstenhorst, S. M., Nothmann, D., Torres-Salazar, D., Hidalgo, P., Schmalzing, G., and Fahlke, C. (2008) Conserved dimeric subunit stoichiometry of SLC26 multifunctional anion exchangers. *J. Biol. Chem.* **283,** 4177–4188

35. Saiyed, T., Paarmann, I., Schmitt, B., Haeger, S., Sola, M., Schmalzing, G., Weissenhorn, W., and Betz, H. (2007) Molecular basis of gephyrin clustering at inhibitory synapses: role of G- and E-domain interactions. *J. Biol. Chem.* **282,** 5625–5632

36. Schmalzing, G., Fallah, G., Detro-Dassen, S., Braam, U., and Markwardt, F. (2010) TMEM16A/anoctamin-1 has a homodimeric architecture. *Protein Science.* (Suppl. 1) **19,** 166

37. Gloor, S., Pongs, O., and Schmalzing, G. (1995) A vector for the synthesis of cRNAs encoding Myc epitope-tagged proteins in *Xenopus laevis* oocytes. *Gene* **160,** 213–217

38. Liman, E. R., Tytgat, J., and Hess, P. (1992) Subunit stoichiometry of a mammalian K^+ channel determined by construction of multimeric cDNAs. *Neuron* **9,** 861–871

39. Nicke, A., Rettinger, J., and Schmalzing, G. (2003) Monomeric and dimeric byproducts are the principal functional elements of higher order P2X$_1$ concatamers. *Mol. Pharmacol.* **63,** 243–252

40. Klapperstück, M., Büttner, C., Böhm, T., Schmalzing, G., and Markwardt, F. (2000) Characteristics of P2X$_7$ receptors from human B lymphocytes expressed in *Xenopus* oocytes. *Biochim. Biophys. Acta.* **1467,** 444–456

41. Becker, D., Woltersdorf, R., Boldt, W., Schmitz, S., Braam, U., Schmalzing, G., and Markwardt, F. (2008) The P2X$_7$ carboxyl tail is a regulatory module of P2X$_7$ receptor channel activity. *J. Biol. Chem.* **283,** 25725–25734

42. Schägger, H., Cramer, W. A., and von Jagow, G. (1994) Analysis of molecular masses and oligomeric states of protein complexes by blue native electrophoresis and isolation of membrane protein complexes by two-dimensional native electrophoresis. *Anal. Biochem.* **217,** 220–230

43. Rosenfeld, J., Capdevielle, J., Guillemot, J. C., and Ferrara, P. (1992) In-gel digestion of proteins for internal sequence analysis after one- or two-dimensional gel electrophoresis. *Anal. Biochem.* **203,** 173–179

44. Beitz, E. (2000) T$_E$Xtopo: shaded membrane protein topology plots in LAT$_E$X2ε. *Bioinformatics* **16,** 1050–1051

45. Das, S., Hahn, Y., Walker, D. A., Nagata, S., Willingham, M. C., Peehl, D. M., Bera, T. K., Lee, B., and Pastan, I. (2008) Topology of NGEP, a prostate-specific cell:cell junction protein widely expressed in many cancers of different grade level. *Cancer Res.* **68,** 6306–6312

46. Wittig, I., Beckhaus, T., Wumaier, Z., Karas, M., and Schägger, H. (2010) Mass estimation of native proteins by blue-native electrophoresis: principles and practical hints. *Mol. Cell. Proteomics.* **9,** 2149–2161

47. Migneault, I., Dartiguenave, C., Bertrand, M. J., and Waldron, K. C. (2004) Glutaraldehyde: behavior in aqueous solution, reaction with proteins, and application to enzyme crosslinking. *BioTechniques* **37,** 790–796, 798–802

48. Leitner, A., Walzthoeni, T., Kahraman, A., Herzog, F., Rinner, O., Beck, M., and Aebersold, R. (2010) Probing native protein structures by chemical cross-linking, mass spectrometry, and bioinformatics. *Mol. Cell. Proteomics.* **9,** 1634–1649

49. Jones, S., and Thornton, J. M. (1996) Principles of protein-protein interactions. *Proc. Natl. Acad. Sci. U.S.A.* **93,** 13–20

50. Wittig, I., Karas, M., and Schägger, H. (2007) High resolution clear native electrophoresis for in-gel functional assays and fluorescence studies of membrane protein complexes. *Mol. Cell. Proteomics.* **6,** 1215–1225

51. Isacoff, E. Y., Jan, Y. N., and Jan, L. Y. (1990) Evidence for the formation of heteromultimeric potassium channels in *Xenopus* oocytes. *Nature* **345,** 530–534

52. Minier, F., and Sigel, E. (2004) Techniques: Use of concatenated subunits for the study of ligand-gated ion channels. *Trends Pharmacol. Sci.* **25,** 499–503

53. Dutzler, R. (2007) A structural perspective on ClC channel and transporter function. *FEBS Lett.* **581,** 2839–2844

54. Dutzler, R., Campbell, E. B., Cadene, M., Chait, B. T., and MacKinnon, R. (2002) X-ray structure of a ClC chloride channel at 3.0 A reveals the molecular basis of anion selectivity. *Nature* **415,** 287–294

55. Marianayagam, N. J., Sunde, M., and Matthews, J. M. (2004) The power of two: protein dimerization in biology. *Trends Biochem. Sci.* **29,** 618–625

56. Jones, D. T. (2007) Improving the accuracy of transmembrane protein topology prediction using evolutionary information. *Bioinformatics* **23,** 538–544